MINERALOGICAL MAGAZINE, SEPTEMBER 1979, VOL. 43, PP. 347-54

Diffuse reflectance spectra and optical properties of some iron and titanium oxides and oxyhydroxides

R. G. J. STRENS[1]

School of Physics, The University, Newcastle upon Tyne NE1 7RU

AND

B. J. WOOD

Department of Geology, The University, Manchester M13 9PL

SUMMARY. The reliability and utility of diffuse reflectance spectra are briefly but critically reviewed. The results of measurements of diffuse reflectance over the wavelength range $200 < \lambda < 2500$ nm are reported for wüstite, magnetite, hematite, maghemite, ilmenite, ulvöspinel, and α-FeO·OH (goethite), β-FeO·OH, γ-FeO·OH (lepidocrocite), and δ-FeO·OH. The spectra have been assigned by reference to simplified molecular-orbital energy-level diagrams derived from recent SCF-Xα calculations.

The specular reflectances reported in the Quantitative Data File (Henry, 1977) are related to the diffuse reflectance spectra in a rational way. Minerals that absorb strongly throughout the visible display little dispersion of specular reflectance, and their powders are dark (wüstite, magnetite, ilmenite, ulvöspinel); those that absorb much more strongly in the near ultraviolet than in the visible have specular reflectances that decrease monotonically from blue to red according to a simple dispersion relation derived by combining the Sellmeier dispersion and Fresnel reflexion equations; their powders are strongly coloured (hematite, maghemite, lepidocrocite, goethite) and their optical anisotropy is closely related to crystal structure.

A KNOWLEDGE and understanding of mineral spectra has both theoretical importance and practical applications. On the one hand, the spectra provide information about the electronic energy levels of the mineral, and these ultimately determine all the physical properties and chemical reactions. On the other hand, the spectra are particularly closely linked with those optical properties that are so widely used in determinative mineralogy. This link between spectra and optics, which is expressed in equations relating the refractive index (n), absorption coefficient (k), and specular reflectance at normal incidence (R), has recently been discussed by Strens and Freer (1978), whose notation is followed here.

The measurement of the transmission spectra of materials that transmit more than about 1% of the incident light through a 30 μm section is comparatively simple, and the spectra of many such minerals are known from near the limit of about 200 nm set by the absorption of air to infra-red wavelengths approaching those of the vibrational absorption beyond about 12 μm (0.1 eV). Much less is known of the spectra of those absorbing phases that are normally studied by reflected light, although with the publication of the Quantitative Data File (QDF) by the Commission on Ore Microscopy (Henry, 1977), specular reflectance data are frequently available for the visible region (400–700 nm), and a few dispersion data (most measured by minimum deviation) are listed in the Landolt-Börnstein (LB) tables (Koritnig, 1962). There are slight differences in composition between our samples and those listed in the QDF and LB tables.

Diffuse reflectance spectroscopy provides a rapid survey technique that locates the main regions of absorption, and provides information on the energy, width, and intensity of absorption bands (Wood and Strens, 1970; Wood, 1971). The spectra described were measured using a Unicam SP700C spectrophometer fitted with the SP735 diffuse reflectance accessory, operating over the wavelength range from 200 to 2500 nm. The reflectance standard was MgO, which was freshly prepared before each series of runs by burning magnesium ribbon. Recorded sample reflectances were converted to absolute values by dividing by the reflectance recorded with MgO in both sample and reference beams.

[1] Present address: Department of Mineralogy and Petrology, Downing Place, Cambridge CB2 3EW.

Diffuse reflectance spectra

Wendlandt and Hecht (1966) have reviewed the theory and practice of diffuse reflectance spectroscopy, and their treatment is followed here. The light reflected by a powder consists partly of light that has been reflected at the surface of the particles, and partly of light that has penetrated the material before being scattered. The former has impressed upon it the specular reflectance spectrum of the material, the latter the transmission spectrum.

In weak absorbers, most of the reflected light has penetrated the sample, and the diffuse reflectance spectrum qualitatively resembles the transmission spectrum of a thin section. The reflectance of the powder is high, that of freshly prepared MgO (which is used as a reflectance standard) being about 98% throughout the visible region.

The diffuse reflectance spectrum of a strong absorber qualitatively resembles the inverted specular reflectance spectrum of the same material, the absolute reflectance being much lower, and typically less than 10%. This is illustrated by platinum, which has a very high specular reflectance of 70% at 589 nm, but which forms 'platinum black' when finely divided.

Many mineral powders display the two types of behaviour in different parts of the spectrum (fig. 1), often being strongly absorbing and weakly reflecting in the near ultraviolet, and weakly absorbing and strongly reflecting in the visible and near infrared. This is illustrated by a number of pigments, of which cinnabar (HgS) is a good example: the powder absorbs strongly in the blue, so that little blue light is reflected. In the red, it is a weak absorber, and (in part because of its high refractive index) displays a very high reflectance. The specular reflectance decreases monotonically from 400 to 700 nm (QDF 1.1620.2).

The assignment of the diffuse reflectance spectra of weak absorbers presents problems similar to those encountered in assigning the transmission spectra of transparent minerals such as olivine, although information on the polarization dependence is lost, and it is difficult to derive absolute absorbances. The interpretation of the spectra of strong absorbers is much more difficult, largely because the specular component of reflexion may dominate at high absorbances, and the ratio of the specular and diffuse contributions is unknown.

Two approaches are possible. The statistical method requires a knowledge of the mean particle diameter and of the refractive index (which may vary rapidly over the wavelength range considered), but given this information the absorption coefficient $k(\lambda)$ may be derived from the observed diffuse reflectance $r(\lambda)$. This method was not practical for our samples, as refractive indices were not known. The second approach is to use the Kubelka–Munk function f(r), which provides a measure of the ratio of the absorption and scattering coefficients. Since the scattering coefficient s is a slowly varying function of wavelength (λ) for grain sizes greater than 2λ, the plot of f(r) provides a good representation of the spectrum. The Kubelka–Munk function is defined by:

$$f(r) = (1-r)^2/2r \simeq k/s \qquad (1)$$

where r is the diffuse reflectance. The presence of a specular component causes k/s to be underestimated at high k, so that the positions and widths of absorption bands are more reliable than their intensities. We have used this method, and all our spectra are presented as plots of f(r) against wavelength (in nm) and photon energy (in eV). In applying the Kubelka–Munk method, certain precautions are necessary. To minimize variations in s, we used grain sizes of >5 μm whenever possible, i.e. more than twice the longest wavelength at which measurements were made. Extreme

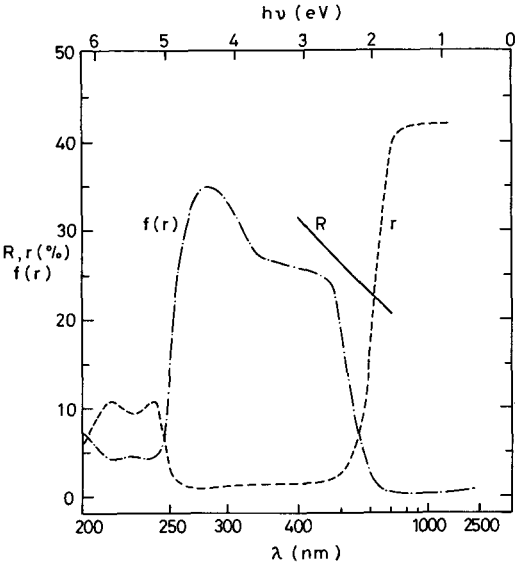

FIG. 1. Relationships between diffuse reflectance (r), specular reflectance (R), and Kubelka–Munk function f(r) in maghemite (γ-Fe_2O_3). Regions of low and high diffuse reflectance are separated by an absorption edge at about 500 nm, which represents the long wavelength limit of an absorption envelope centred at $\bar{\lambda} = 336$ nm. The f(r) spectrum shows inverse variation with r, with f(r) becoming very sensitive to small changes in the absolute value of r as $r \to 0$, so that values of f(r) above about 50 (for which $r \simeq 1\%$) are unreliable. The specular reflectance shows normal dispersion ($R_{blue} > R_{red}$, $dR/d\lambda$ negative) for $\lambda > \bar{\lambda}$, but reverse dispersion ($dR/d\lambda$ positive) is expected for $\lambda < \bar{\lambda}$, with small or irregular dispersion near $\bar{\lambda} = 336$ nm.

distortion of spectra, with the generation of spurious absorption bands, may occur when dealing with a physical mixture of two phases of different properties, or a crystal having highly anisotropic absorbances: this is because the spectrum is always dominated by light reflected by the less absorbing phase, so that the changes caused by a strong absorption band in one phase (or orientation) may be swamped by quite minor variations in the reflectance of the other. Finally, the apparent positions of absorption bands in reflectance spectra (both specular and diffuse), are shifted from their real positions, i.e. the band positions in $r - \lambda$ or $f(r) - \lambda$ spectra are not the same as those in $k - \lambda$ plots. Our work is thus a reconnaissance rather than a definitive survey of the spectra, and it is likely that later and more detailed results will disagree with ours in some respects.

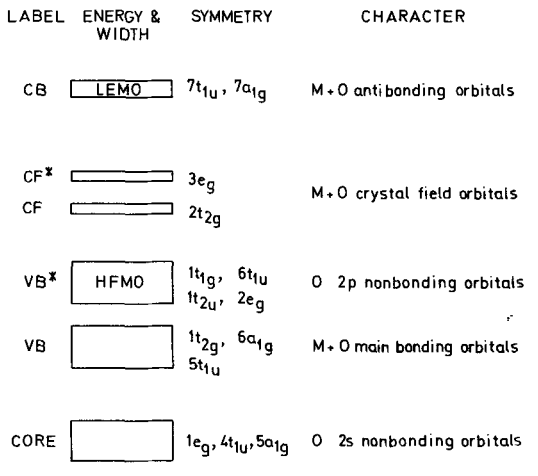

FIG. 2. Generalized molecular orbital energy level diagram for $3d^n$ ions with $0 < n < 10$, based on calculations by Tossell *et al.* (1974) for Ti^{4+}, Fe^{3+}, and Fe^{2+} ions octahedrally coordinated by oxygen. The widths and relative energies of the orbitals are indicated, but both width and spacing vary from ion to ion. The core–VB and VB–CB separations are 10 to 15 and 10 to 20 eV, respectively.

The lowest empty molecular orbitals (LEMO) of a d^{10} ion are those of the conduction band (CB). The highest full molecular orbitals (HFMO) of a d^0 ion are the oxygen 2*p* non-bonding orbitals of the valence band (VB*). Between these lie the 3*d* (crystal field or CF and CF*) orbitals, which are empty for n = 0, full for n = 10, and otherwise partially filled. The CF–CF* separation (Δ) of about 1.2 eV gives rise to weak absorption near 1000 nm in compounds containing octahedral $Fe^{2+}(d^6)$. The onset of strong absorption by oxygen → metal charge transfer (VB*–CF) is at about 3 eV, 3.5 eV, and 4.3 eV for $Ti^{4+}(d^0)$, $Fe^{3+}(d^5)$, and $Fe^{2+}(d^6)$, respectively (Tossell *et al.*, 1974). The width of the first major absorption band is typically 2–3 eV.

Transition energies and intensities

Recent SCF-Xα calculations (Tossell *et al.*, 1973, 1974; Tossell, 1978) have elucidated the molecular-orbital energy-level schemes of Fe^{2+}, Fe^{3+}, and Ti^{4+} octahedrally coordinated by oxygen. In discussing the results, previous workers have usually emphasized the bonding, non-bonding, or antibonding nature of the orbitals (which affect such properties as stability and hardness) rather than properties of spectroscopic importance. The spectroscopist is primarily concerned with the occupancy (full, half-filled, empty) of the orbitals, and their energies, character (*s*, *p*, *d*) and symmetry, as these are the properties that determine transition energies and intensities.

The calculations reveal many similarities between the molecular-orbital energy levels of the common transition-metal ions, and a generalized summary of the main features is shown in fig. 2. The orbitals are conveniently grouped into bands of broadly similar character, thus the $1e_g$, $4t_{1u}$, and $5a_{1g}$ orbitals are close in energy, and have little *p* or *d* character, all being derived from oxygen 2*s* atomic orbitals. These orbitals hold a very tightly bound group of core electrons, and have a small radial extent. By contrast, the diffuse $7a_{1g}$ and $7t_{1u}$ orbitals occur at low binding energies, and probably form a conduction band. Between these extremes lie the $3e_g$ and $2t_{2g}$ crystal field bands, which are narrow in energy and usually partly filled (but empty in d^0 and full in d^{10} ions), and the main orbitals of the valence band, formed from the oxygen 2*p* atomic orbitals, but having significant metal 4*s* and 3*d* content.

The intensities of the electronic transitions responsible for light absorption are governed by a number of selection rules. The Pauli exclusion principle forbids transitions between filled levels, and obviously no transition can occur between empty levels. The Laporte selection rule allows only those transitions in which the subsidiary quantum number (l) changes by ± 1, i.e. *s*–*p*, and *p*–*d* but not *s*–*s*, *p*–*p*, *d*–*d*. or *s*–*d* transitions. This rule is often relaxed sufficiently (e.g. by mixing some *p* character into orbitals of *d* character) to allow weak transitions such as the *d*–*d* bands responsible for the colour of many minerals. The spin selection rule forbids transitions in which there is a change in spin multiplicity, and there are also symmetry constraints on the transition probabilities, and thus on the band intensities, with g↔g and u↔u transitions forbidden and g↔u allowed.

Applied to fig. 2, these considerations imply that the core levels at high binding energies will contribute only to absorption in the far ultraviolet near 15–20 eV (70 nm). There will be a region of low

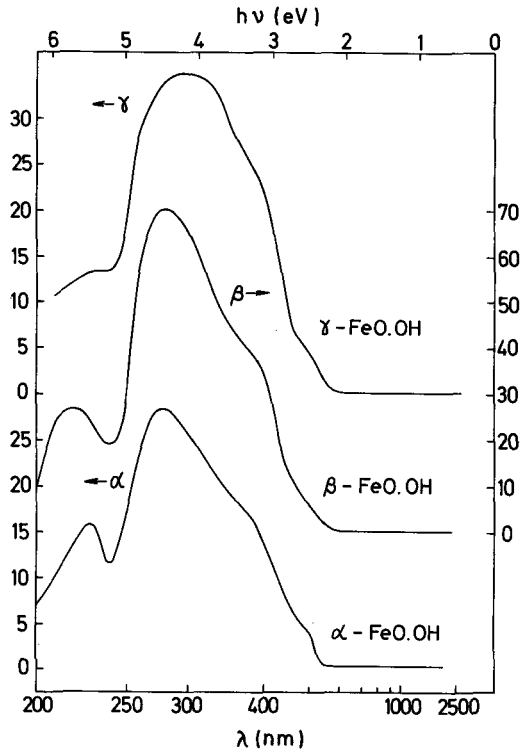

FIG. 3. Diffuse reflectance spectra of α-, β- and γ-FeO·OH, showing the variation of $f(r) \simeq k/s$ as defined in equation (1) with wavelength and photon energy. The main absorption centred at 275–97 nm is assigned to $O \rightarrow Fe^{3+}$ charge transfer (VB*–CF). The arrows indicate the $f(r)$ scale to be used for each spectrum.

absorption extending from the vibrational absorption below 0.1 eV (12 μm) to about 3 eV (400 nm) in which only weak Laporte-forbidden *d–d* transitions will occur. In the near ultraviolet, strong transitions will occur between the valence band (VB) and crystal field (CF) levels, and between the crystal field and conduction band (CB) levels at energies of about 3–6 eV (400 to 250 nm), and others will occur between the valence and conduction bands at energies above about 9 eV (140 nm). The optical properties (particularly dispersion and bireflectance or birefringence) in the visible region will be determined mainly by the VB*–CF and CF or CF*–CB transitions.

Spectra and optics

Minerals in the system Fe–Ti–O–H display a wide range of optical properties. Iron is metallic; ilmenite, ulvöspinel, magnetite, and wüstite are opaque non-metals; hematite, maghemite, and the FeO·OH phases are strongly coloured, and the three TiO_2 polymorphs are transparent. The optical properties of opaque non-metals, strongly coloured materials, and transparent phases are related to their spectra through equations (5*a*, 5*b*), (9), and (6*b*) of Strens and Freer (1978).

The properties of the transparent minerals are not considered here, as their refractive indices in the visible region are well represented by the Sellmeier dispersion equation, and their reflectances can be calculated from the indices using Fresnel reflexion equation. Metals contain free electrons and require a different approach. We have therefore confined our attention to the strongly coloured and the opaque but non-metallic phases in the system.

Strongly coloured phases

The FeO·OH *phases.* Goethite (α) and lepidocrocite (γ) are the iron analogues of the AlO·OH minerals diaspore and boehmite, while β-FeO·OH is not a true oxyhydroxide, but an analogue of hollandite in which the molecular water occupies large interstices. Iron is octahedrally coordinated in the α, β, and γ forms, but the δ-FeO·OH structure is based on sheets of (O,OH) ions in hexagonal close packing, with about 80% of the iron in octahedral and 20% in tetrahedral positions.

The four FeO·OH phases are used as pigments, and the spectra of commercial samples manufactured by the Mapico Carbon Co. were recorded without further treatment. All have broadly similar spectra (fig. 3), each spectrum having a region of relatively low absorption and high r for $\lambda > 500$ nm, with very high absorption and low r below 400 nm. The original spectra show weak features at 965 (α) and 995 (γ), and at about 700 nm, attributable respectively to the $^6A_1$–$^4T_1$ and $^6A_1$–$^4T_2$ transitions of octahedrally coordinated Fe^{3+}.

The spectra of α-, β-, and γ-FeO·OH show strong absorption at about 290 nm, with a weaker resolved band at about 230 nm. The spectrum of δ-FeO·OH (fig. 4) displays a broad band system centred at 330 nm, with a well-resolved feature at 217 nm. The SCF-Xα calculations of Tossell *et al.* (1974) and Tossell (1978) suggest that these bands may confidently be assigned to transitions between the oxygen non-bonding and metal *d*-orbitals (VB* to CF). The polarized specular reflectance spectra of lepidocrocite (QDF 1.4840) and goethite (QDF 1.3180) display a monotonic variation of R with wavelength from 300 to 700 nm. The reflectance is quite well represented by the equation:

$$R(\%) = 100\ \{(1 + IL/\pi^2)^{\frac{1}{2}} - 1\}^2 / \{(1 + IL/\pi^2)^{\frac{1}{2}} + 1\}^2$$

$$\text{where } L = \lambda^2/(\lambda^2 - \lambda_i^2) \qquad (2)$$

derived by substituting the Sellmeier expression for

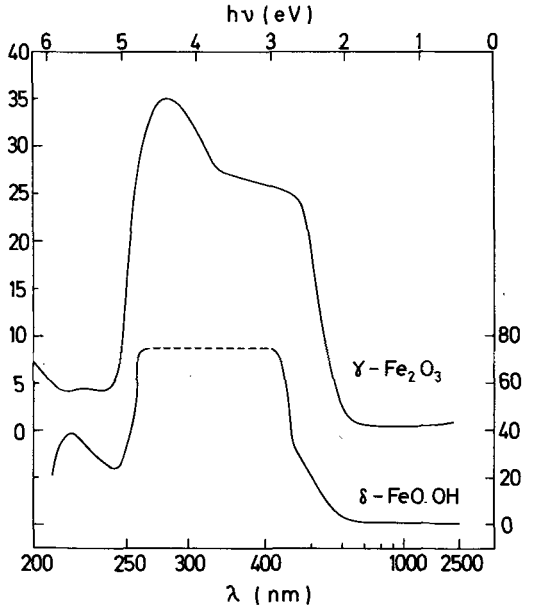

FIG. 4. Diffuse reflectance spectra of maghemite (γ-Fe_2O_3) and δ-FeO·OH, both of which contain octahedral and tetrahedral Fe^{3+}, showing the variation of $f(r) \simeq k/s$ with wavelength and photon energy. The absorption envelope centred at about 330 nm arises from VB*-CF transitions of both octahedral (Tossell *et al.*, 1974) and tetrahedral (Tossell, 1978) ferric iron. Values of $f(r)$ are unreliable where dashed.

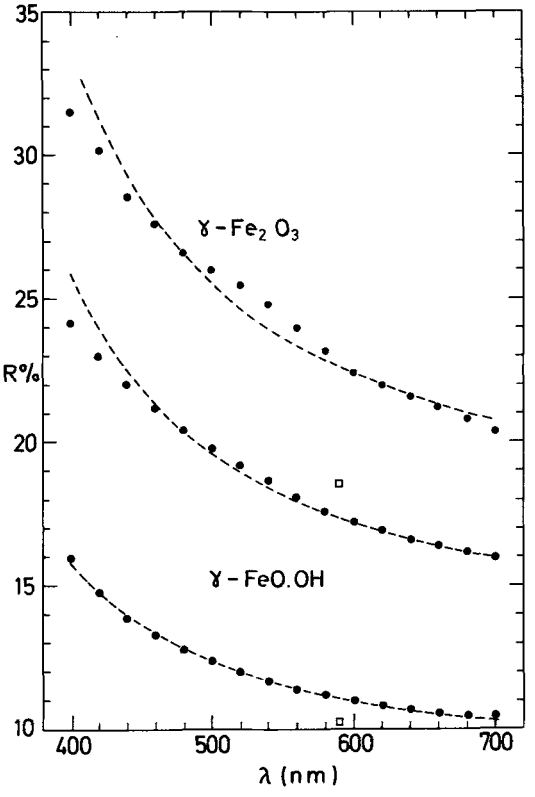

FIG. 5. The observed specular reflectances (●) of maghemite (top) and lepidocrocite $R(\alpha')$ and $R(\gamma')$ are plotted at 20 nm intervals from 400 to 700 nm. The dashed line shows the values calculated using equation (2) with the Sellmeier constants (I_i, λ_i) derived from reflectances at 475 and 625 nm. Reflectances calculated from the observed α and γ indices of lepidocrocite using the Fresnel equation are also shown (□).

n into the Fresnel reflexion equation (fig. 5). The Sellmeier constants (I_i, λ_i) are given in Table I. Better agreement should be achieved using equation (9) of Strens and Freer (1978) but this requires a knowledge of the absorption band parameters (a_i, w_i, λ_i) which we do not yet possess.

Goethite and lepidocrocite are sufficiently well crystallized and transparent in the red and yellow to permit measurement of indices by minimum deviation. Goethite, although orthorhombic, is nearly uniaxial with $\alpha \| [010] = 2.30$, $\beta \simeq \gamma \simeq 2.44$ (LB 174). Lepidocrocite has extreme birefringence, with $\alpha \| [010] = 1.941$, $\beta \| [001] = 2.20$, $\gamma = 2.515$ (LB 174). The α index of goethite is normal to the (100) layers of h.c.p. (O,OH) ions and to the octahedral strips $\|$ [001]. In lepidocrocite, γ correlates with the axis of the octahedral chains, β with the direction in which these chains are cross-linked to form sheets, and α with the normal to the (010) c.c.p. anion layers. Values of λ_i deduced from the dispersion data range from 237–52 nm (goethite) to 314 nm for the γ index of lepidocrocite: they compare well with $\bar{\lambda} = 275$ and 297 nm respectively.

Hematite and maghemite. Hematite was prepared by sintering pellets of Mapico high purity Fe_2O_3 at 1100 °C for 8 h in air. Synthetic maghemite (Pfizer) was used as received. Iron is octahedrally coordinated in hematite, but maghemite (a defect spinel structure) has approximately 5/8 of the cations in tetrahedral and 3/8 in octahedral coordination.

The hematite spectrum (fig. 6) qualitatively resembles those of α-, β-, and γ-FeO·OH, with a strong absorption envelope centred at 370 nm, partially resolved into four components at 230, 280, 370, and 510 nm, which are again assigned to $O \rightarrow Fe^{3+}$ (VB* to CF) transitions. The $^6A_{1g}$–$^4T_{1g}$ band lies at 870 nm. The specular reflectance of hematite (QDF 1.3640) decreases smoothly from 32.6 (ω) and 28.9 % (ε) at 400 nm, to 24.9 and 21.8 % at 700 nm. The reflectances deviate increasingly from the values calculated from equation (2) as the region of high absorption is approached.

TABLE I. *Dispersion of indices and specular reflectance: the Sellmeier constants of strongly coloured phases*

		λ_1 (nm)	λ_2 (nm)	n_1, R_1	n_2, R_2	I	λ_i	$\bar{\lambda}$
Goethite	α	542	850	2.303	2.185	34.35	237.0	—
	β	542	850	2.439	2.292	38.29	251.9	—
	γ	542	850	2.447	2.304	38.89	248.3	—
								275
	$R_{\alpha'}$	400	700	23.6	15.7	35.8	285	—
	$R_{\gamma'}$	400	700	19.9	14.2	33.0	261	—
Lepidocrocite	γ	589	671	2.515	2.425	37.62	314.0	—
								297
	$R_{\alpha'}$	400	700	24.2	16.0	36.5	287	—
	$R_{\gamma'}$	400	700	16.0	10.4	23.5	272	—
Hematite	ω	656	760	3.042	2.904	56.85	360.6	—
	ε	656	760	2.797	2.690	49.18	340.7	
								370
	R_o	400	700	32.6	24.9	66.8	270	—
	R_e	400	700	28.9	21.8	55.5	265	—
Maghemite	R	400	700	31.5	20.4	48.0	305	336

n_1, R_1 and n_2, R_2 are the indices (LB) and specular reflectances (QDF) at wavelengths λ_1, λ_2; I_i and λ_i are the Sellmeier constants calculated from the experimental (n, R) using equation (6*b*) of Strens and Freer (1978) and equation (2) above; $\bar{\lambda}$ is the estimated position of the centre of the near ultraviolet absorption envelope in the diffuse reflectance spectra.

With the exception of hematite R_o and R_e, there is satisfactory agreement between the values of integrated absorbance (I_i) and wavelength (λ_i) deduced from indices, reflectance, and spectra.

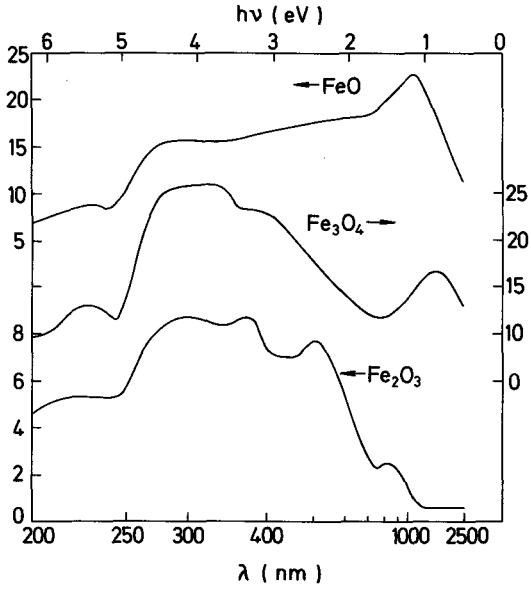

FIG. 6. Diffuse reflectance spectra of wüstite, magnetite, and hematite. For assignments see text. The arrows indicate the f(r) scale to be used.

Dispersion data (LB 174) include $\omega = 3.042$, $\varepsilon = 2.797$ at 656 nm, and yield $\lambda_i = 361$ (ω) and 341 nm (ε), which compare with the value of $\bar{\lambda} = 370$ nm for the centre of the near-ultraviolet band system (Table I). The optical anisotropy ($\omega > \varepsilon$) probably reflects the greater degree of polyhedral linkage $\perp c$ resulting from the presence of (0001) h.c.p. oxygen layers. Each pair of Fe^{3+} ions shares a face in the c-direction, but a total of six edges and six corners $\perp c$.

The maghemite spectrum (fig. 4) is dominated by a strong absorption band centred at 336 nm and containing at least two components, the stronger peaking at 280 nm: it qualitatively resembles that of δ-FeO·OH which also contains both tetrahedral and octahedral Fe^{3+} ions. The assignment is again to $O \rightarrow Fe^{3+}$ (VB*-CF) transitions. The specular reflectance of maghemite (QDF 1.5140) decreases smoothly from 31.5 to 20.4% between 400 and 700 nm, the lower dispersion and reflectance of maghemite being attributable to the difference in position of the near-ultraviolet absorption (maghemite $\bar{\lambda} = 336$ nm, hematite $\bar{\lambda} = 370$ nm).

Opaque phases

Wüstite. Wüstite was prepared by sintering a mixture of Mapico high purity Fe_2O_3 and iron sponge (Johnson Matthey) in an iron crucible at 1100 °C overnight. A diffractometer scan confirmed that the product was wüstite with a defect NaCl structure, and a composition near $Fe^{2+}_{0.87}Fe^{3+}_{0.09}O$.

The spectrum displays a sharp absorption band

at 946 nm (fig. 6), which may confidently be assigned to a *d–d* transition of octahedral Fe^{2+}. Strong absorption with maxima at about 230 and 280 nm is assigned to VB*–CF transitions, which are predicted to occur at energies above 4 eV (300 nm). The unexpectedly high absorption at about 2.5 eV may be caused by a charge-transfer process involving Fe^{2+} and Fe^{3+} ions, although the energy is rather high for this (Smith and Strens, 1976). Another possibility is that the absorption is caused by a spin-forbidden *d–d* transition the intensity of which is enhanced by magnetic coupling between Fe^{2+} and Fe^{3+} ions (Smith, 1978).

Specular reflectance data for wüstite (QDF 1.9840) reveal a shallow minimum at 470 nm (18.1 %), rising to 18.9 at 400 nm and 19.6 at 700 nm. This non-dispersive behaviour is typical of materials that absorb strongly and nearly uniformly throughout the visible region.

Magnetite. Magnetite was prepared by heating pellets of a stoichiometric mixture of hematite and reduced iron sponge at 1100 °C *in vacuo* overnight. A diffractometer scan confirmed the purity of the product.

Above the Verwey transition at 120 K, magnetite has one Fe^{3+} ion on the tetrahedral position (Fe–O = 1.89 Å), and two indistinguishable iron atoms on the octahedral positions (Fe–O = 2.06 Å). This is the result of electron hopping on a time scale short compared with that of the atomic vibrations, so that the octahedral sites are effectively occupied by $Fe^{2.5+}$ rather than Fe^{2+} and Fe^{3+}.

The magnetite spectrum (fig. 6) resembles those of hematite and the FeO·OH phases apart from a band at 1400 nm, between the energies expected for *d–d* transitions of octahedral (1.15 eV, 1080 nm) and tetrahedral (0.75 eV, 1650 nm) Fe^{2+}. We tentatively assign this to a charge-transfer process between octahedral ions. The main absorption envelope represents VB*–CF transitions of both octahedral and tetrahedral ions.

The specular reflectance (QDF 1.5220.2) varies only from 19.7 to 21.1 % over the visible in keeping with the strong absorption throughout the 400–700 nm region.

Ilmenite and ulvöspinel. Ilmenite and ulvöspinel were prepared by heating pellets of stoichiometric mixtures of TiO_2, reduced iron sponge and hematite *in vacuo* overnight. Phase purity was confirmed by diffractometer scans.

The spectra (fig. 7) show an absorption feature in both minerals at 1000 nm attributable to the t_{2g}–e_g transition of octahedral Fe^{2+}. Absorption by $O \rightarrow Fe^{2+}$ charge transfer (VB*–CF) is expected at < 300 nm, and $O \rightarrow Ti$ charge transfer at < 400 nm, leaving the strong absorption at 500 nm to be accounted for. We provisionally assign this to

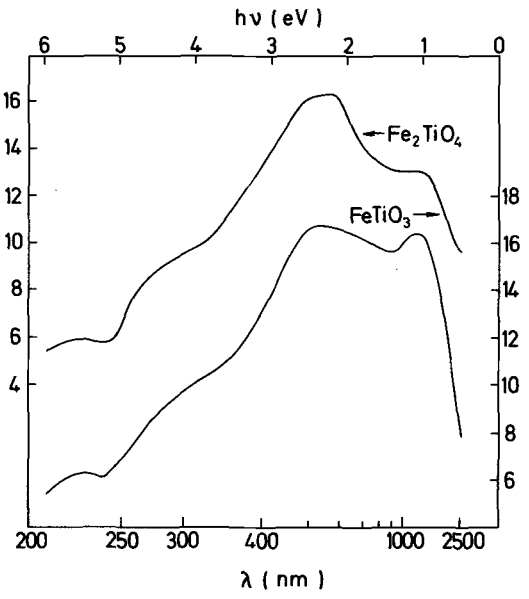

FIG. 7. Diffuse reflectance spectra of ulvöspinel and ilmenite. Bands at about 1 and 2.25 eV are assigned to *d–d* transitions of octahedral Fe^{2+} and to $Fe^{2+} \rightarrow Ti^{4+}$ charge transfer respectively. Absorption at higher energies is attributed to $O \rightarrow Ti$ and $O \rightarrow Fe$ charge transfer (VB* to CF). The arrows indicate the f(*r*) scale to be used.

$Fe^{2+} \rightarrow Ti^{4+}$ charge transfer, which is known to occur at similar energies in other minerals (Smith and Strens, 1976).

As in wüstite, the presence of strong absorption throughout the visible region results in small dispersion of reflectance, which varies only from 14.9 to 17.7 % in ulvöspinel (QDF 1.9280) and from 20.0 to 21.2 % in ilmenite (QDF 1.4020).

Discussion and conclusion

The optical properties of the iron and titanium oxides and oxyhydroxides are related to their spectra and structures in a rational way. The opaque but non-metallic phases (ilmenite, ulvöspinel, magnetite, and wüstite) absorb strongly throughout the visible region, have dark powders, and display little dispersion of reflectance. By contrast, the strongly coloured phases exhibit strong dispersion of index and reflectance, both *n* and *R* decreasing monotonically from 400 to 700 nm in accordance with the Sellmeier dispersion and Fresnel reflexion equations, although marked deviations between calculated and observed reflectances occur as the region of high absorption is reached.

The dispersion of the indices and reflectances of

the strongly coloured phases depends mainly upon the wavelength of the main near-ultraviolet absorption envelope, increasing as λ_i approaches the visible. Optical anisotropy (birefringence and bireflectance) in these phases results from structural control of the λ_i, with the directions of highest (λ_i, n, R) correlating with the axes of chains or strips (goethite) or the planes of sheets (lepidocrocite) of metal-oxygen polyhedra. The lowest index is frequently normal to the planes of oxygen closest packing (goethite, lepidocrocite, hematite), and the mode of linkage of polyhedral elements (faces, edges, corners) is also important in determining the λ_i and thus the optical anisotropy, the general rule being that cross-linking increases λ_i.

REFERENCES

Henry (N. F. M.), ed., 1977. Quantitative Data File of the IMA-COM. McCrone, London.

Koritnig (S.), 1962. In *Landolt-Börnstein Zahlenwerte und Funktionen*, II Band, 8 Teil (Optische Konstanten). Springer-Verlag, Berlin.

Smith (G.), 1978. *Phys. Chem. Minerals*, **3**, 375.

——and Strens (R. G. J.), 1976. *In* Strens (R. G. J.), ed. *The Physics and Chemistry of Minerals and Rocks*. Wiley, London and New York.

Strens (R. G. J.) and Freer (R.), 1978. *Mineral. Mag.* **42**, 19.

Tossell (J. A.), 1978. *Phys. Rev.* B, **17**, 484.

——Vaughan (D. J.), and Johnson (K. J.), 1973. *Nature Phys. Sci.* **244**, 42.

————————1974. *Am. Mineral.* **59**, 319.

Wendlandt (W. W.) and Hecht (H. G.), 1966. *Reflectance Spectroscopy*. Wiley, London and New York.

Wood (B. J.), 1971. Ph.D. thesis, University of Newcastle upon Tyne.

——and Strens (R. G. J.), 1970. Abstracts, IMA-IAGOD Meeting (Tokyo), 116.

[*Manuscript received 6 April 1979*]